Preparation and Characterization of Nano SiO_2 for Bioactive Glasses Application through High Energy Ball Milling

Annamalai MAHENDRAN [1] *, Annamalai JEGAN [2]

[1] *Department of Mechanical Engineering, Sona College of Technology, Salem-636005, Tamil Nadu, India*
[2] *Department of Mechanical Engineering, Selvam College of Technology, Namakkal- 637003, Tamil Nadu, India*

http://doi.org/10.5755/j02.ms.39486

Received 27 November 2024; accepted 8 April 2025

Bioactive glasses 58S in the SiO_2-CaO-P_2O_5 combination have been successfully employed as bone-filling materials in orthopedic and dental surgery, but their low mechanical strength limits their utilization in load-bearing positions. Various methods for the synthesis of bio-glass and its composites have been explored to present, including traditional melt quench, flame synthesis, sol-gel, and microwave irradiation. Various groups have looked at bio glass synthesis. These synthesis methods are relatively successful, however they have a high preparation cost. In order to lower the expense of preparation, Bio-active glass compositions will indeed be Nano sized, which will improve bonding ability with lowering production costs. In this present study, Nano-sized silicon dioxide powder was manufactured through ball milling in order to achieve the best possible combination between mechanical and biological attributes. The key benefit is that by machining, the density is also lowered. It provides extra assistance in mixing and connecting with other particles. The nano silicon dioxide is produced by ball milling at varied rotational speeds like 100 rpm, 200 rpm, and 300 rpm with two different durations as 2 and 4 h. The six nanopowder samples were obtained and densities were analyzed with TEM, XRD and SEM for each samples. This study proved, based on the aforementioned observations, that the proposed ball milling method for nanoparticle production is capable which would be significantly beneficial in the manufacturing of bioactive glasses.

Keywords: bioactive glass, silicon dioxide, ball milling, TEM, SEM, nanoparticle.

1. INTRODUCTION

Many clinical conditions addressed by orthopedic and dental medicine necessitate bone repair. The gold standard is an autogenously bone graft, but host tissue is typically sparse and difficult to model to the shape required for effective reconstruction [1]. The public's focus was then shifted to implantation. Although bioactive ceramics have had remarkable success in bone healing, their elastic modulus mismatch and stress shielding of human bone cannot keep up with the increasing lifespans. Tissue engineering offers a novel method to address these issues. The biomaterials should serve as a framework to aid or increase the body's inherent ability to repair itself [2].

Silica (SiO_2) is a key component in the production of bio glass 58S, as well as in the ceramics sector, where it is used as a principal component in applications such as bottles, cement, electronics, paints, ceramics, glass, industrial tires, and even cosmetics [3]. SiO_2@YVO4:Yb3+, Er3+ microspheres with a core-shell structure were synthesized and characterized by Liang et al [4]. Microspheres were created using the simple sol-gel method and a heating step. The samples were evaluated using photoluminescence spectra and Fourier transforms infrared spectroscopy. The results then show that the SiO_2 spheres were effectively covered with YVO4:Yb3+, Er3+ phosphors to produce core-shell structures, and the size distribution of the resulting microspheres is uniform. This SiO_2@YVO4:Yb3+, Er3+ microspheres with a core-shell structure could be extremely useful for infrared detection and display technology.

Using a top-down technique and ultrafine grinding, Agus et al [5] produced nanoparticle silica using quartzite and silica sand. When samples are leached with sulfuric acid at room temperature, their good SiO_2 value of 98 % rises to 99.7 %. The high-grade silica was subsequently ground many times in a planetary ball mill. The ideal outcome was achieved in 30 to 50 h of grinding, resulting in nanoparticles of silica measuring 80 nm in size. According to TEM analysis, this nanoparticle appears to have aggregated as a typical milling product, which was brought on by Van der Walls' force between the particles following the milling process. The formation of a fine Si-based powder that spontaneously reacts with water at room temperature to rapidly and efficiently produce hydrogen has been studied by Xu et al [6]. They found that when Si is ball-milled under inert conditions in the presence of KOH and sucrose, a fine Si-based powder is produced. They claimed that under aerobic conditions, Si powder that has been ball-milled and embedded with KOH can react with many types of water, including tap water, river water, and salt water, to form H_2. This technique offers a low-cost, scalable method for providing tiny fuel cells with hydrogen fuel safely. Girija et al. used to compare the development of porous-structured Akermanite ($Ca_2MgSi_2O_7$) using ball milling, sol-gel, and hybrid processes for orthopedic applications. They compared the mechanochemical synthesis process to

* Corresponding author: A. Mahendran
E-mail: *mahendrana@sonatech.ac.in*

traditional procedures such as sol-gel synthesis and ball milling, and found that it performed better [7].

Eikeland et al [8] evaluated metallurgical grade silicon manufactured by a planetary ball mill, and based on the ideas from the stress model; they looked at the properties of the powder as a function of grinding duration, grinding bead size, and rotational speed. With a constant specific energy input to the mill, the powder was produced using 2 mm grinding beads and 4 h of grinding. With the exception of the particle size distribution, a lower rotational speed produced a powder that was comparable. Mutlu et al [9]'s creation of SiO_2-CaO hollow mesoporous bioactive glass nanoparticles for bone applications used etching and impregnation processes. Nanoparticles are significant because they naturally have a higher surface-to-volume ratio than bigger particles. These large surface areas have the potential to enhance interfacial driven phenomena including wetting and adhesion as well as catalytic reactions. Regarding the nanoparticles' internal structure, it has been discovered that nanocrystalline materials outperform their microcrystalline counterparts in terms of hardness, fracture toughness, and low temperature ductility.

Ruchi et al [10] have researched the sol-gel synthesis of silicon dioxide and have a fundamental grasp of how the calcination temperature affects the growth of silicon dioxide produced by the hydrolysis of TEOS with ethanol, deionized water, and a catalyst mixture. SEM, X-ray diffraction (XRD), AFM, and photoluminescence were used to investigate the characteristics of the resultant materials, as well as their optical properties (PL). Hench et al [11] have studied a layer of hydroxyapatite that can grow on the surface of bioactive glass (BG), specifically 45S5 (45 wt.% SiO_2, 24.5 wt.% CaO, 24.5 wt.% Na_2O, and 6wt percent P_2O_5), which is being researched for usage in biological applications. According to Azizi et al [12] electrophoretic deposition is a workable technique for the co-deposition of Na-Alg and bioglass nanoparticles, which can be utilized to create a variety of magnesium alloy coatings with customized microstructures and surfaces for use in biomedicine. In the system of P_2O_5-CaO-Na_2O-SiO_2-TiO_2 via the sintering process, Seyedsahameddin et al [13] have explored phosphate-based-glass ceramics. Different concentrations of these elements were doped in the parent glass in place of calcium oxide in order to assess the effects of strontium and zinc. Scanning electron micrographs reveal that after three days of simulated bodily fluid (SBF) soaking, hydroxyapatite nuclei formed on the surfaces of the samples. However, after 28 days, the substrate's breakdown caused the nuclei to dissolve in the solution.

The melting process of multicomponent bioactive glass (0Z, 46SiO_2-30CaO-18Na_2O-6P_2O_5, wt. percent) has been studied by Fengjie Li et al [14] by employing ball-milling to combine YSZ and 0Z particles, the 5Y bioactive glass-ceramic is created. The authors propose that this technique for making good bioactive glass-ceramic is a contender (5Y) for clinical applications requiring load bearing. Several methods have been used to manufacture silicon dioxide. For use in microelectronics, optical, electrical, and other disciplines, it is highly desirable to synthesize crystalline and homogeneous materials. Sol-gel technology has been widely applied [15].

The synthesis of bio-glass and its composites has so far been accomplished using a number of techniques, such as microwave irradiation, sol-gel, traditional melt quench, and flame synthesis. Numerous groups have reviewed the production of bioactive glass, and while the synthesis techniques used are rather efficient, they are also expensive to produce [16 – 18]. To overcome it and reducing the cost of preparation Bio-active glass composition are to be Nano sized after that the bonding ability also increasing and cost wise low. In this experimental work, Nano-sized silicon dioxide powder was manufactured through ball milling in order to achieve the best possible combination between mechanical and biological attributes by reduction of manufacturing cost and time.

2. EXPERIMENTAL METHODS

2.1. Ball milling process

In this experimental work Fritsch high energy ball mill machine have been used to produce silicon dioxide nano powder. The machine has tempered steel grinding bowl with capacity of 250 ml, and machine shown in Fig. 1. To begin experimental, we must operate the high energy ball milling machine for 10 min on sand to clean the balls and bowl. Following that, the balls and the basin completely cleaned with tissue paper and acetylene solution. In this experimental work three levels of speed were taken with two different time of duration and shown in Table 1.

Fig. 1. Ball milling machine

For the experimental work, the silicon dioxide of 35 g of six samples pack were taken for each run. Each run of silica powder is poured into the bowl of the high energy ball milling machine.

Table 1. Ball milling parameters levels

Run No.	Running speed, rpm	Duration, h
1	100	2
2	100	4
3	200	2
4	200	4
5	300	2
6	300	4

In high energy ball mill machine 6 numbers of tungsten balls were put on the bowl. First run of experiment was done with 100 rpm of speed for 2 h all the run numbers were operated as per the Table 1. Silicon dioxide nanopowder of each run was collected and then characterization was done for particle analyze.

2.2. Characterization

A Hitachi H-800 transmission electron microscope (TEM) with a voltage of 150 kV was used to obtain TEM pictures. A JEOL JEM-2100 TEM with a field emission gun operating at 200 kV was used to perform high resolution transmission electron microscopy (HRTEM). A very helpful approach is X-ray diffraction (XRD), which uses the diffraction pattern of a radiation beam to assist in identifying the crystal structure. Similar to how light be diffracted from a grate, beam diffraction only occurs in a few distinct directions [19, 20]. Such a pattern yields crystal structure information. In the current study, X-ray diffraction analysis of the as-synthesized product containing SiO_2 nanostructures was carried out using an XRD (Bruker AXS, Model-D8 Advance) with a Cu k (= 1.5402) X-ray source in the 2 range of 20 – 80 degrees that was functioned at 40 kV and 30 mA.

The scanning electron microscope (SEM) is a type of electron microscope that creates images of a material by scanning the surface with a concentrated stream of electrons. The sample's atoms and electron interactions produce a diverse range of signals that provide characteristics on the sample's surface topography and composition. In most applications, data are gathered over a predetermined region of the sample's surface, and a 2-dimensional image is created to show the spatial variations in these characteristics. In this experimental study, standard SEM equipment from CARL ZEISS (USA), Sigma with Gemini Column, and EDAX Bruker (German) Nano XFlash Detectors were used with an area magnification ranging from 20X to around 30,000X, and a spatial resolution of 50 to 300 nm.

3. RESULTS AND DISCUSSION

3.1. X-ray diffraction

Fig. 2 depicts the crystallite size for various parameters. The outcomes of an XRD examination on powder form are depicted in Fig. 3. Using the Debye-Scherer equation and these graphs [21, 22], we may calculate the size of the sub-micrometer particles or crystallites, as shown below:

$$D = 0.9\lambda / \beta cos\ \theta\ , \quad (1)$$

where λ is the wavelength of X-ray beam (λ=1.5406 Å); θ is the Braggs angle; β is the full width at half maximum (FWHM) of the intense peak [23, 24].

The synthesis of SiO_2 powder by ball milling process with different parameters setup was carried out and their samples were examined by XRD diffraction. Based on the XRD diffraction procedure for six samples, the 2theta and FWHM are listed in below Table 2. We can be certain that the substance generated is SiO_2 (Quartz) nanoparticles by comparing the XRD spectrum we obtained for SiO_2. Fig. 3 a shows the XRD analysis for SiO_2 six samples and it reveals that at a height of intensity 4342 a.u the SiO_2 particle has been achieved 2 theta value of 32.08º with the FWHM value of 0.1938 for the running of ball mill 100 rpm with the duration of 2 h. The ball mill running of 300 rpm with 4 h duration was given the 2 theta value of 32.17º with the peak height of intensity is 5197 and exposed in Fig. 3 f. Estimate the size of the particles among all six samples we can use the aforementioned Eq. 1 and the calculated SiO_2 particle size are enumerated in Table 2. From the Table 2, it is clear that the ball milling parameters 200 rpm with 2 h has provided a better crystallite size of 38.66 nm than other combinations of ball milling parameters.

Table 2. Calculation of SiO_2 crystallite size

Ball milling parameters	2θ, º	FWHM, º	Crystallite size, nm
100 rpm – 2 h	32.08339	0.19338	44.65
100 rpm – 4 h	32.01308	0.17985	48.01
200 rpm – 2 h	32.06185	0.22335	38.66
200 rpm – 4 h	32.19783	0.19296	44.75
300 rpm – 2 h	32.23108	0.2021	42.73
300 rpm – 4 h	32.17276	0.19681	43.89

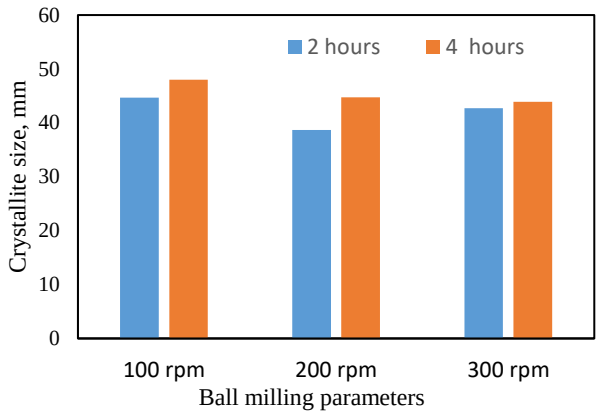

Fig. 2. Crystallite size for various parameters

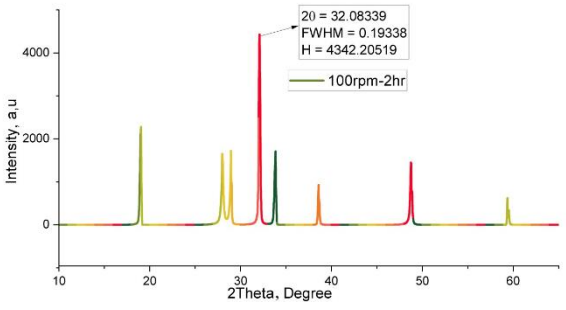

a

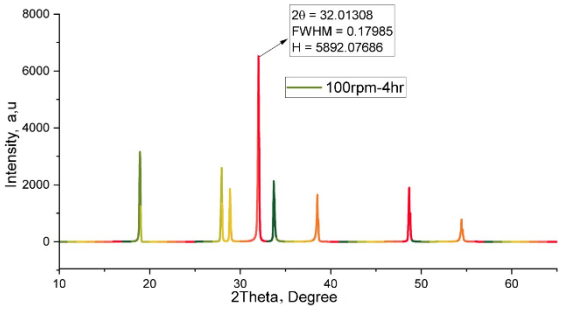

b

continued on next page

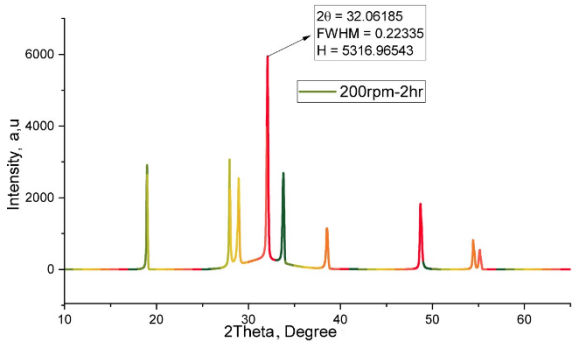

c

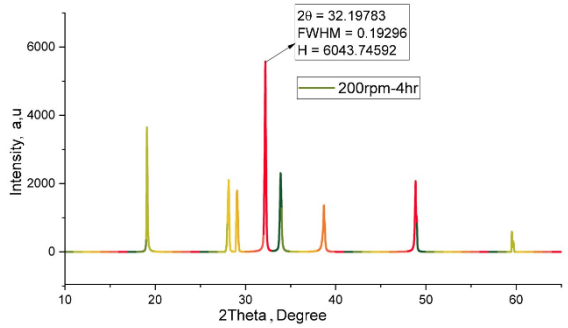

d

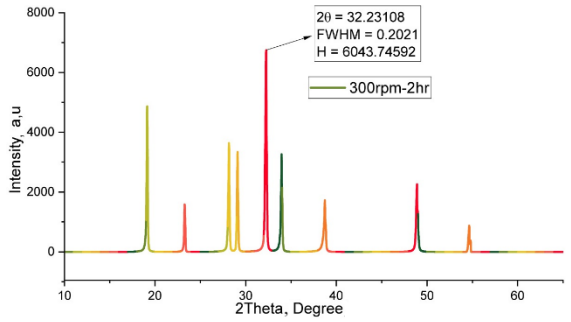

e

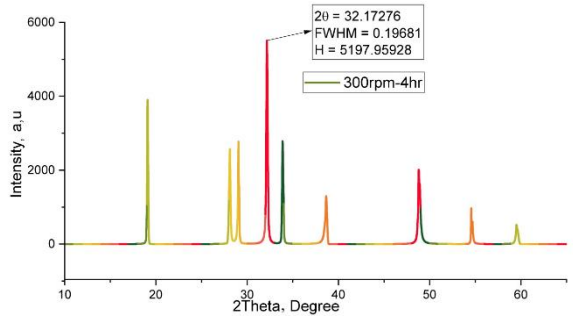

f

Fig. 3. XRD patterns of SiO_2: a – at 100 rpm 2 h; b – at 100 rpm 4 h; c – at 200 rpm 2 h; d – at 200 rpm 4 h; e – at 300 rpm 2 h; f – at 300 rpm 4 h

3.2. Transmission electron microscopic analysis

Transmission Electron Microscopic (TEM) was used at various magnifications to further analyze the microstructure of the SiO_2 samples. Scanning the images at low magnification levels is mostly done to check for micron-sized nanoparticle adherence in the samples. It is therefore hard to see the existing clusters in Nano pictures at magnifications of 50.000 and higher if nanoparticles transformed into micro-size cluster by adhesion in this situation. A maximum magnification of 1.200.000 was used to capture the TEM pictures shown in Fig. 4 with a 1 µm index [24, 25].

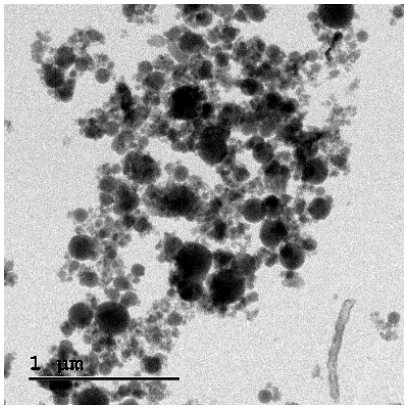

a

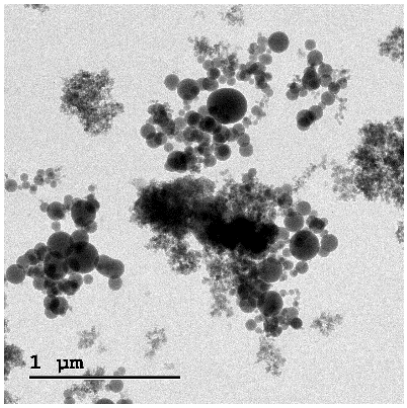

b

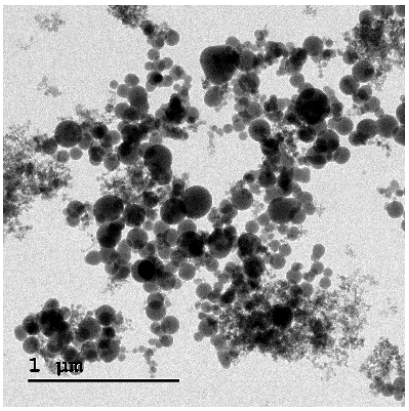

c

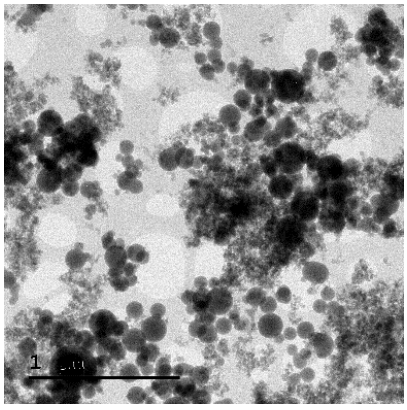

d

continued on next page

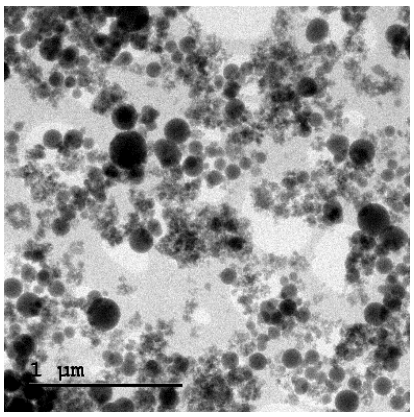

e

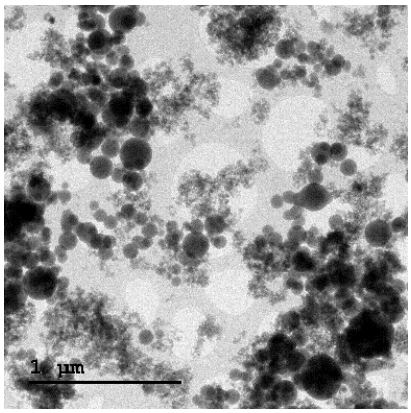

f

Fig. 4. Transmission electron microscopic images of SiO_2: a – at 100 rpm 2 h; b – at 100 rpm 4 h; c – at 200 rpm 2 h; d – at 200 rpm 4 h; e – at 300 rpm 2 h; f – at 300 rpm 4 h

All of the particles in the samples had a different size, according to TEM pictures of the original nanoparticles. This demonstrates that, practically, the "adhesion" process does not occur in the 100 rpm with 2 h and 100 rpm 4 h samples and shown in Fig. 4 a and b. In addition, the experimental sample consists SiO_2 nanoparticles with clear shape and size, each of which has a diameter of 40 nm for 200 rpm with 2 h ball milling parameter and shown in Fig. 4 c. Additionally, by examining the TEM pictures in Fig. 4 d, e, and f, we can conclude that neutron irradiation causes the generation of new nanoparticles with an average size of 50 nm in the material with "adhesion" for 200 rpm with 4 h, 300 rpm with 2 h and 4 h ball milling parameters. As can be seen from Fig. 4 d and f, while the ball milling process is running at a fast speed, the temperature inside the drum is dispersed, and as a result, the particles are more likely to stick together. Furthermore, the electrophysical properties of the nanomaterial are directly impacted by this slight "adhesion." Six samples of SiO_2 particles were analyzed using TEM, and it was found that the nominal speed of the ball milling process, 200 rpm, for two hours would produce the best size of Nano SiO_2 particles with a distinct shape [26].

3.3. Scanning electron microscope analysis

A scanning electron microscope (SEM) was used to analyze the morphology of the nanopowder. SEM pictures of SiO_2 nanoparticles captured during the tests at a 100 KX magnification and 200 nm indexes are displayed in Fig 5.

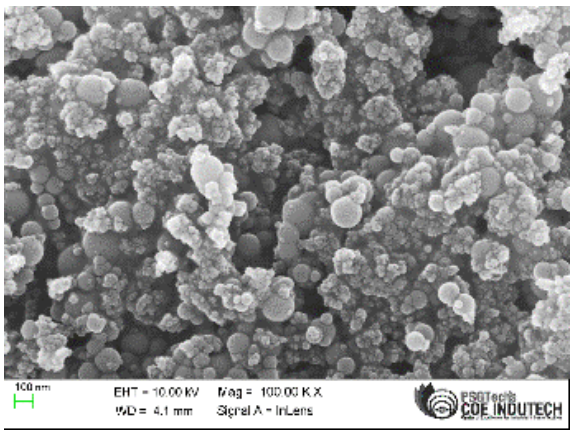

a

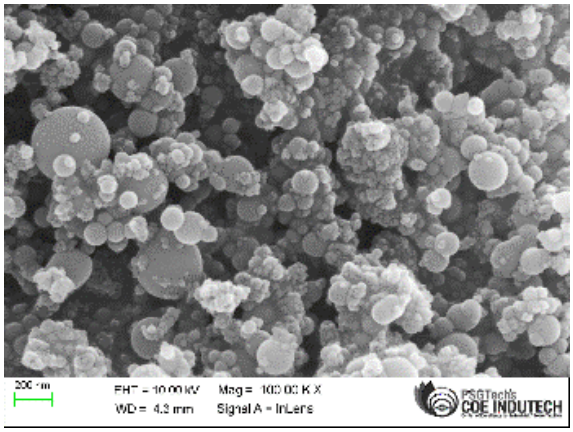

b

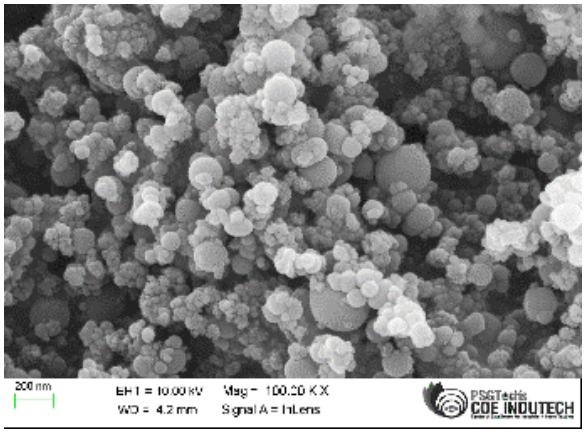

c

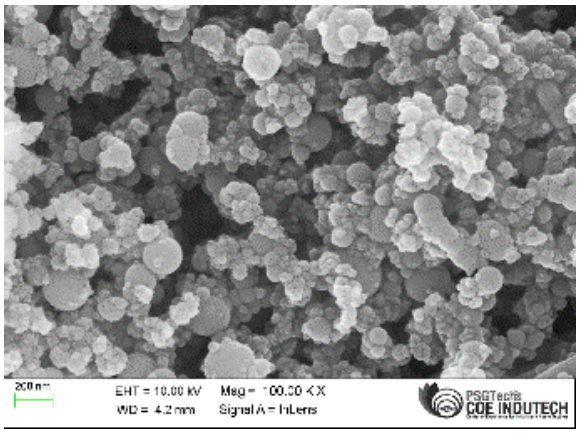

d

continued on next page

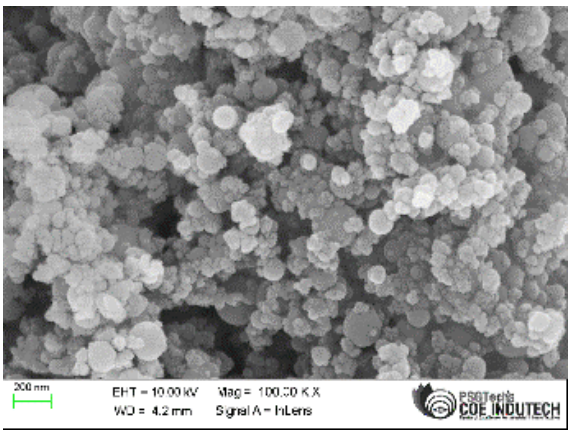

e

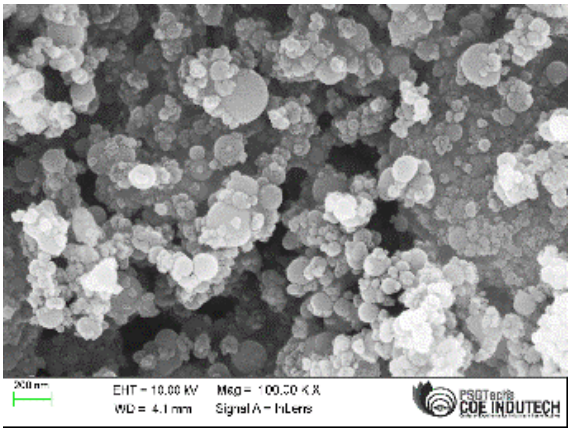

f

Fig. 5. Scanning electron microscopic image of SiO_2: a – at 100 rpm 2 h; b – at 100 rpm 4 h; c – at 200 rpm 2 h; d – at 200 rpm 4 h; e – at 300 rpm 2 h; f – at 300 rpm 4 h

The major goal of scanning the images in low magnification order is to see how the nanoparticles adhere to one another in the samples. According to the SEM pictures in Fig. 5 a, a wide spread of nanoparticles with adhesion between them is produced when 100 rpm is applied for a two-hour period. It is also noted that the SiO_2 nanoparticles are not distributed uniformly. Fig. 5 b depicts the SEM picture for a sample that was subjected to a 4 h ball milling process at 100 rpm. It shows how the neutron flux has caused the particles to transform into large-size "combinations" (clusters). The SEM pictures of the ball milling processes at 200 rpm for 4 h, 300 rpm for 2 h, and 300 rpm for 4 h are revealed in Fig. 5 d, e, and f, respectively. It is obvious that the highest adhesion between nanoparticles is caused by increasing temperature concerning increasing ball milling speed and time duration [27, 28]. In Fig. 5 c, it is shown that the nanoparticles were disseminated uniformly and without adhesion during a 2 h ball milling process at a speed of 200 rpm. This particular combination of manufacturing parameters was more effective at producing nanosize silica particles than others.

To examine the clusters that can form in several hundred nanometers, let's now review pretty high magnification. The investigations showed that the sample maintained its amorphous characteristics both before and after irradiation, indicating that the sample had not changed its condition. As a result of general analyses of the nanoparticles, it is now known that SiO_2 nanoparticles exhibit macro- or micro-size "adhesion" due to the highest inside the bowl as the process's duration increases [29, 31].

A particle size analyzer (PSA) was used to measure the size of the nano SiO_2 for bioactive glasses. The analyzer's graph showed that the peak was between 10 and 100 nm, with the average mean size of the SiO_2 100 rpm with 2 h and 100 rpm with 4 h nanoparticles being 28.07 nm and 15.20 nm, respectively. Similarly, the average mean size of the SiO_2 200 rpm with 2 h and 200 rpm with 4 h nanoparticles being 36 nm and 18.05 nm, respectively. Then the average mean size of the SiO_2 300 rpm with 2 h and 300 rpm with 4 h nanoparticles being 27.39 nm and 20.22 nm, respectively. This suggested the presence of the nano SiO_2 for bioactive glasses particles revealed in Fig. 6 a – f. It validates the nano-size based on PSA analysis; nano SiO_2 for bioactive glasses particles ranged in size from 20 to 30 nm, with an average of 25 nm [32]. According to Qiu H. et al. [33], it is also acknowledged that the shape and size of nanoparticles affect their absorption. Likewise, nanomaterials' optical characteristics can be altered based on their shape, size, and other characteristics.

Fig. 7 demonstrates the various sizes and shape of the nano SiO_2 for bioactive glasses. A TEM image of the nano SiO_2 sample's particle sizes as a representative composite of the entire group is shown in Fig. 7 a – f. This figure illustrates that this composite is situated in the nanoscale region, with a significant agglomeration and a mean particle size of 25 nm [26]. This indicates the modifications in the composite nanopowders' morphology. Our study efforts on the final result of the various running speeds with various hours of the nanoparticles will be detailed in the forthcoming paper.

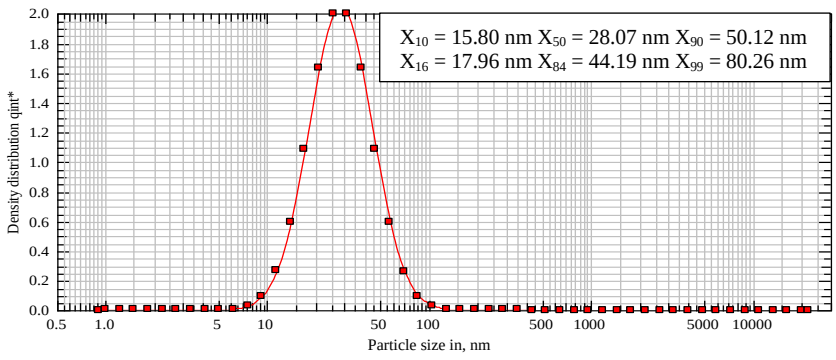

a

continued on next page

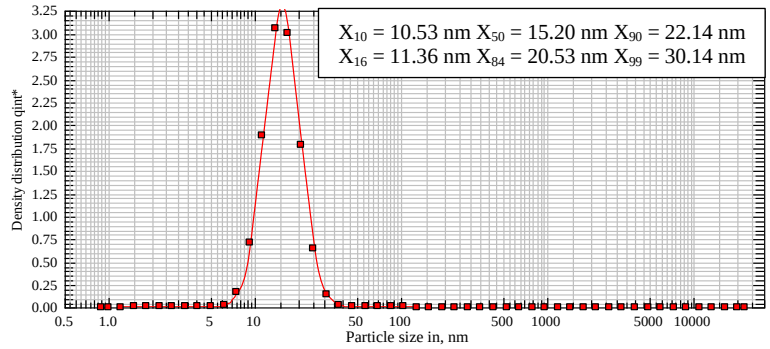

b

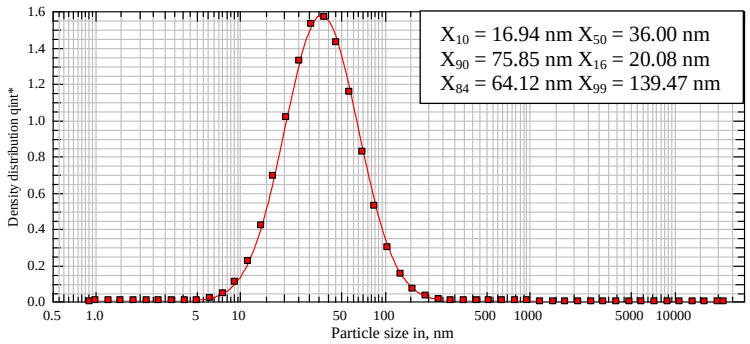

c

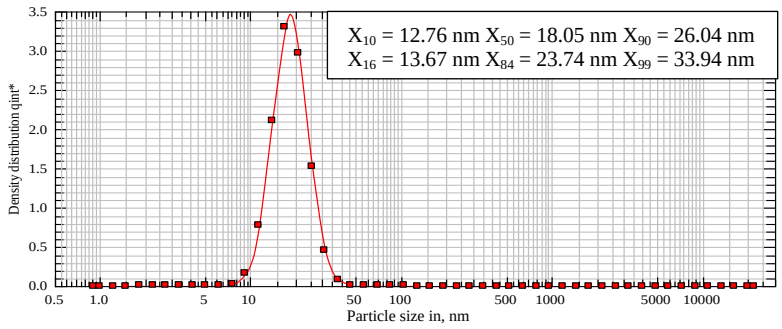

d

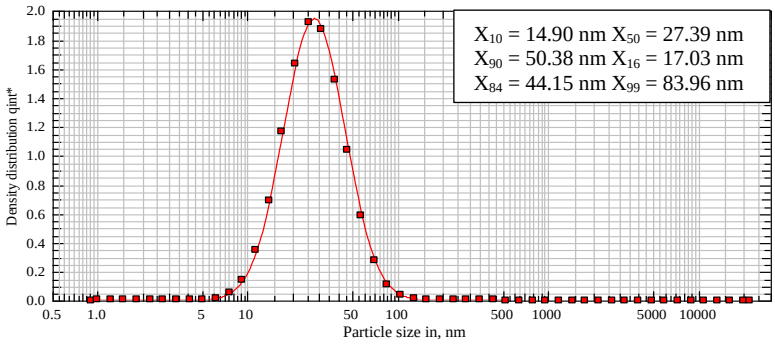

e

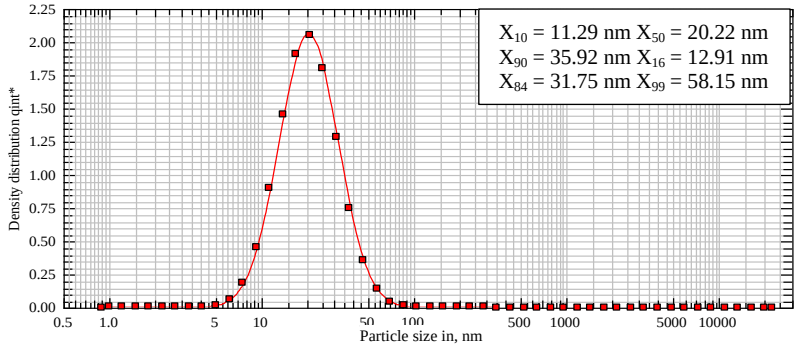

f

Fig. 6. Particle size analysis of SiO_2: a – at 100 rpm 2 h; b – at 100 rpm 4 h; c – at 200 rpm 2 h; d – at 200 rpm 4 h; e – at 300 rpm 2 h; f – at 300 rpm 4 h

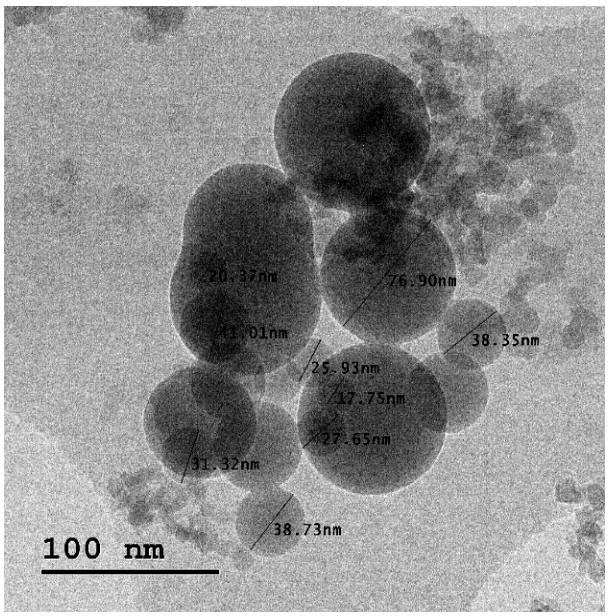

a

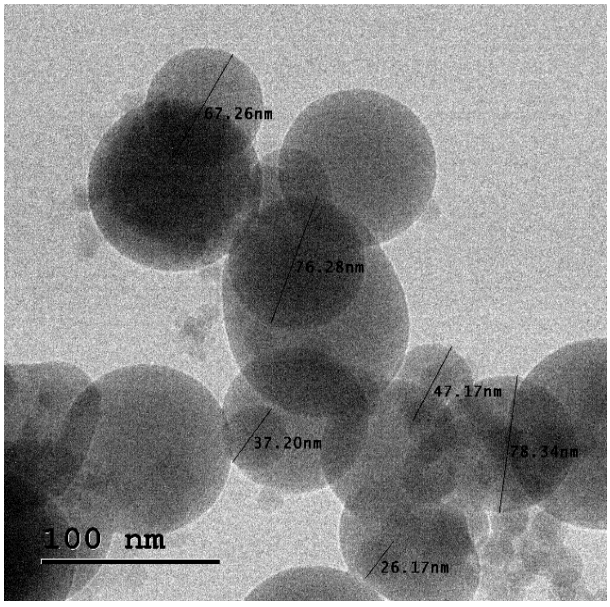

b

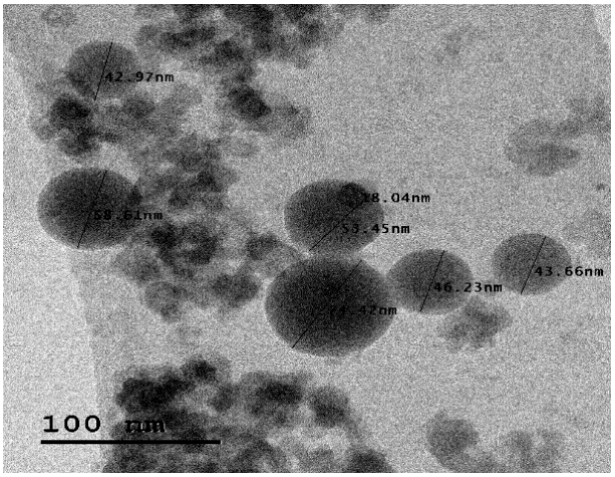

c

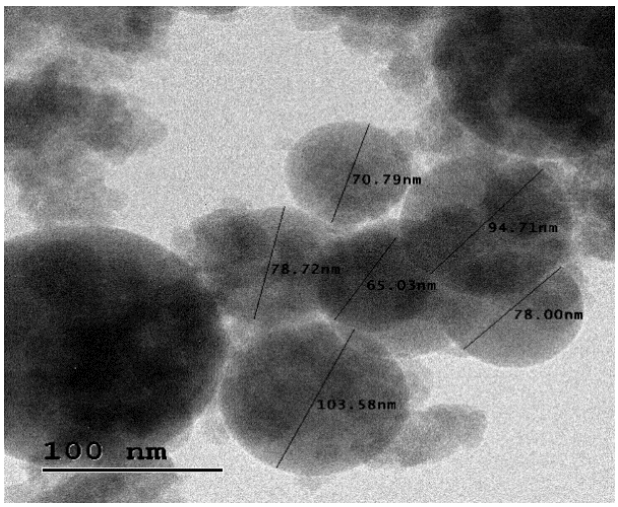

d

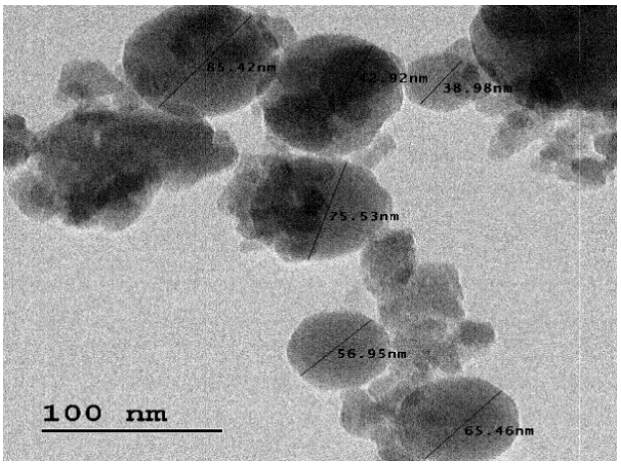

e

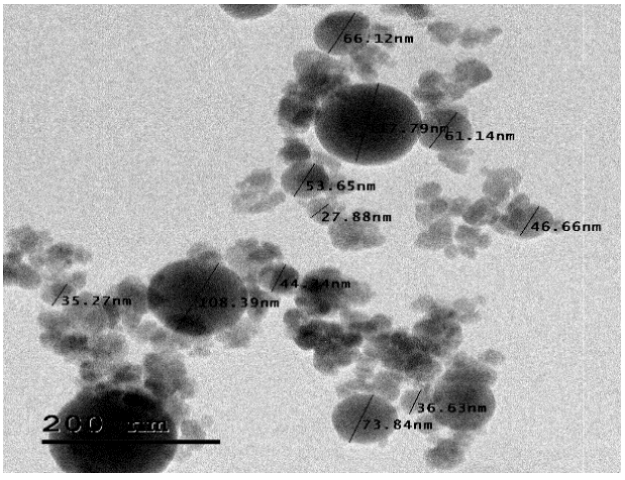

f

Fig. 7. TEM images of nano SiO_2: a – at 100 rpm 2 h; b – at 100 rpm 4 h; c – at 200 rpm 2 h; d – at 200 rpm 4 h; e – at 300 rpm 2 h; f – at 300 rpm 4 h

4. CONCLUSIONS

The primary scientific and technological objective of this work was to create an easy, lab-based approach for producing SiO_2 powder for Bioactive glasses 58S. Simple ball milling with six distinct milling parameter setups has been successful in producing crystalline silica. The samples

have undergone TEM, XRD, and SEM analysis in order to establish the crystalline structure of nanomaterial at low Nano sizes. It has been discovered through TEM examinations of Nano SiO_2 samples for six different ball milling parameters that there is very little "adhesion" seen at small dimensions under the ball milling process has a higher rpm rate because of the high temperature.

1. Consistent to the XRD results, the produced silica exhibits crystalline phase features with an average crystallite size of about 39 nm, which is smaller than that of other samples that were subjected to different ball milling parameters.
2. According to the results of this investigation, the ball milling parameters of 200 rpm rotation for a 2 h period will produce SiO_2 particles of a better size than other parameter setups.
3. Conferring to SEM examinations of nano-SiO_2 samples, nanoparticles do not "adhesion" when ball milling speed is set to a very low level over a medium period of time.
4. However, it is evident from SEM investigations that the modest amount of "adhesion" significantly impacts the electro physical properties of nanomaterials as a result of the ball milling process' increasing speed and duration. For the production of SiO_2 particles for bioactive glasses 58S, it has been observed that the ball milling process is an easy and efficient way. In order to examine the clusters that can form in several hundred nanometers, let's now review pretty high magnification. The investigations showed that the sample maintained its amorphous characteristics both before and after irradiation, indicating that the sample had not changed its condition.

REFERENCES

1. **Auregan, J.C., Begue, T.** Bioactive Glass for Long Bone Infection: A Systematic Review *Injury* 46 (8) 2015: pp. S3 – S7. https://doi.org/10.1016/S0020-1383(15)30048-6
2. **Bui, X.V., Dang, T.H.** Bioactive Glass 58S Prepared Using an Innovation Sol-Gel Process *Processing and Application of Ceramics* 13 (1) 2019: pp. 98 – 103. https://doi.org/10.2298/PAC1901098B
3. **Palakurthy, S., Reddy, K.V., Patel, S., Azeem, P.A.** A Cost Effective SiO_2–CaO–Na_2O Bio-Glass Derived from Bio-Waste Resources for Biomedical Applications *Progress in Biomaterials* 9 2020: pp. 239 – 248. https://doi.org/10.1007/s40204-020-00145-0
4. **Liang, Y., Ouyang, J., Wang, H., Wang, W., Chui, P., Sun, K.** Synthesis and Characterization of Core–Shell Structured SiO_2@ YVO_4: Yb3+, Er3+ Microspheres *Applied Surface Science* 258 (8) 2012: pp. 3689 – 3694. https://doi.org/10.1016/j.apsusc.2011.12.006
5. **Agus, W., Teguh, N., Siti, R.** Preparation of Nanoparticle Silica from Silica Sand and Quartzite by Ultrafine Grinding *Proceeding of International Conference* 28 2012: pp. 1 – 7.
6. **Xu, L., Ashraf, S., Hu, J., Edwards, P.P., Jones, M.O., Hadzifejzovic, E., Foord, J.S.** Ball-Milled Si Powder for the Production of H2 From Water for Fuel Cell Applications *International Journal of Hydrogen Energy* 41 (30) 2016: pp. 12730 – 12737. https://doi.org/10.1016/j.ijhydene.2016.05.181
7. **Girija, M., Kumar, T.S.** A Comparative Investigation on The Development of Porous-Structured Akermanite ($Ca_2mgsi_2o_7$) Via Ball Milling, Sol-Gel, and Combination (Hybrid) Process for Orthopedic Applications *Journal of Materials Research* 39 (15) 2024: pp. 2198 – 2214. https://doi.org/10.1557/s43578-024-01378-6
8. **Nilssen, B.E., Kleiv, R.A.** Silicon Powder Properties Produced in A Planetary Ball Mill as A Function of Grinding Time, Grinding Bead Size and Rotational Speed *Silicon* 12 (10) 2020: pp. 2413 – 2423. https://doi.org/10.1007/s12633-019-00340-0
9. **Mutlu, N., Beltrán, A.M., Nawaz, Q., Michálek, M., Boccaccini, A.R., Zheng, K.** Combination of selective Etching and Impregnation Toward Hollow Mesoporous Bioactive Glass Nanoparticles *Nanomaterials* 11 (7) 2021: pp. 1846. https://doi.org/10.3390/nano11071846
10. **Nandanwar, R., Singh, P., Haque, F.Z.** Synthesis and Characterization of Sio2 Nanoparticles by Sol-Gel Process and Its Degradation of Methylene Blue *American Chemical Science Journal* 5 (1) 2015: pp. 1 – 10. https://doi: 10.9734/ACSj/2014/10875
11. **Hench, L.L.** The Future of Bioactive Ceramics *Journal of Materials Science: Materials in Medicine* 26 (86) 2015: pp. 1 – 4. https://doi.org/10.1007/s10856-015-5425-3
12. **Azizi Amirabad, A., Allahkaram, S.R.** Electrochemical Behavior of Nanostructured Bioglass®/Alginate Composite Coating on Magnesium Alloy by Electrophoretic Deposition for Orthopedic Application *Journal of Ultrafine Grained and Nanostructured Materials* 55 (1) 2022: pp. 49 – 57. https://doi.org/10.22059/JUFGNSM.2022.01.08
13. **Razavi, S., Yekta, B.E., Khavandi, A.** Effect of SrO and ZnO on Densification and in Vitro Behaviors of P_2O_5-CaO-Na_2O-SiO_2-TiO_2 Bioactive Glass-Ceramics *Sustainable Chemical Engineering* 2022: pp. 49 – 65. https://doi.org/10.37256/sce.3120221228
14. **Li, F., Jiang, Y., Chen, M., Yu, B., Wang, J., Wang, F.** Effect of ZrO_2 Addition on In-vitro Bioactivity and Mechanical Properties of SiO_2–Na_2O–CaO–P_2O_5 Bioactive Glass-Ceramic *Ceramics International* 48 (13) 2022: pp. 18541 – 18550. https://doi.org/10.1016/j.ceramint.2022.03.124
15. **Rahman, I.A., Padavettan, V.** Synthesis of Silica Nanoparticles by Sol-Gel: Size-Dependent Properties, Surface Modification, and Applications in Silica-Polymer Nanocomposites – A Review *Journal of Nanomaterials* 2012 (1) 2012: p. 132424. https://doi.org/10.1155/2012/132424
16. **Angioni, D., Orrù, R., Cao, G., Garroni, S., Bellucci, D., Cannillo, V.** Bioactivity Enhancement by A Ball Milling Treatment in Novel Bioactive Glass-Hydroxyapatite Composites Produced by Spark Plasma Sintering *Journal of the European Ceramic Society* 43 (3) 2023: pp. 1220 – 1229. https://doi.org/10.1016/j.jeurceramsoc.2022.10.077
17. **Erol-Taygun, M., Zheng, K., Boccaccini, A.R.** Nanoscale Bioactive Glasses in Medical Applications *International Journal of Applied Glass Science* 4 (2) 2013: pp. 136 – 148. https://doi.org/10.1111/ijag.12029
18. **Nandanwar, R., Singh, P., Haque, F.Z.** Synthesis and Characterization of SiO_2 Nanoparticles by Sol-Gel Process and its Degradation of Methylene Blue *American Chemical Science Journal* 5 (1) 2015: pp. 1 – 10. http://dx.doi.org/10.9734/ACSJ/2015/10875

19. **Gauna, M.R., Conconi, M.S., Suarez, G., Aglietti, E.F., Rendtorff Birrer, N.M.** Dense Zircon ($ZrSiO_4$) Ceramics by a Simple Milling-Sintering Route *Science of Sintering* 50 2018: pp. 15 – 28. https://doi.org/10.2298/SOS1801015G
20. **Gauna, M.R., Martinez, J.M., Conconi, M.S., Suárez, G., Rendtorff, N.M.**. Effect of TiO2 in Fine Zircon Sintering and Properties *Science of Sintering* 53 (2) 2021: pp. 267 – 283. https://doi.org/10.2298/SOS2102267G
21. **Leenakul, W., Tunkasiri, T., Tongsiri, N., Pengpat, K., Ruangsuriya, J.** Effect of Sintering Temperature Variations on Fabrication of 45s5 Bioactive Glass-Ceramics Using Rice Husk as a Source for Silica *Materials Science and Engineering: C* 61 2016: pp. 695 – 704. https://doi.org/10.1016/j.msec.2015.12.029
22. **Holzwarth, U., Gibson, N.** The Scherrer Equation Versus the' Debye-Scherrer Equation' *Nature Nanotechnology* 6 (9) 2011: pp. 534 – 534. https://doi.org/10.1038/nnano.2011.145
23. **Klug, H.P., Alexander, L.E.** X-Ray Diffraction Procedures: For Polycrystalline and Amorphous Materials 1974: pp. 992.
24. **Stokes, A.R., Wilson, A.J.C.** A Method of Calculating the Integral Breadths of Debye-Scherrer Lines *In Mathematical Proceedings of the Cambridge Philosophical Society* 38 (3) 1942: pp. 313 – 322. https://doi.org/10.1017/S0305004100021988
25. **Kargozar, S., Baino, F., Banijamali, S., Mozafari, M.** Synthesis and Physico-Chemical Characterization of Fluoride (f)-and Silver (ag)-Substituted Sol-Gel Mesoporous Bioactive Glasses *Biomedical Glasses* 5 (1) 2019: pp. 185 – 192. https://doi.org/10.1515/bglass-2019-0015
26. **Abulyazied, D.E., Alturki, A.M., Youness, R.A., Abomostafa, H.M.** Synthesis, Structural and Biomedical Characterization of Hydroxyapatite/Borosilicate Bioactive Glass Nanocomposites *Journal of Inorganic and Organometallic Polymers and Materials* 31 2021: pp. 4077 – 4092. https://doi.org/10.1007/s10904-021-02070-6
27. **Langford, J.I., Wilson, A.J.C.** Scherrer After Sixty Years: A Survey and Some New Results in the Determination of Crystallite Size *Journal of Applied Crystallography* 11 (2) 1978: pp. 102 – 113. https://doi.org/10.1107/S0021889878012844
28. **Taha, M.A., Youness, R.A., Zawrah, M.F.** Phase Composition, Sinterability and Bioactivity of Amorphous Nano-Cao-Sio2-Cuo Powder Synthesized by Sol-Gel Technique *Ceramics International* 46 (15) 2020: pp. 24462 – 24471. https://doi.org/10.1016/j.ceramint.2020.06.231
29. **Ghosh, T.K., Chakrabarti, S.K., Ghosh, S., Saha, S., Dey, S., Das, S.K.** Synthesis, Characterization, Bioactivity and Cytotoxicity Assessment of Nano Zro_2 Reinforced Bioactive Glass Ceramics *Ceramics International* 49 (20) 2023: pp. 32694 – 32710. https://doi.org/10.1016/j.ceramint.2023.07.237
30. **Angioni, D., Orrù, R., Cao, G., Garroni, S., Bellucci, D., Cannillo, V.** Bioactivity Enhancement by A Ball Milling Treatment in Novel Bioactive Glass-Hydroxyapatite Composites Produced by Spark Plasma Sintering *Journal of the European Ceramic Society* 43 (3) 2023: pp. 1220 – 1229. https://doi.org/10.1016/j.jeurceramsoc.2022.10.077
31. **Wang, H., Zhao, S., Cui, X., Pan, Y., Huang, W., Ye, S., Luo, S., Rahaman, M.N., Zhang, C., Wang, D.** Evaluation of Three-Dimensional Silver-Doped Borate Bioactive Glass Scaffolds for Bone Repair: Biodegradability, Biocompatibility, and Antibacterial Activity *Journal of Materials Research* 30 (18) 2015: pp. 2722 – 2735. https://doi.org/10.1557/jmr.2015.243
32. **Krishnand, S.I., Tariq, A.S., Nazir, A.B., Faroog, A.A., Jagan, C.S., Faheemn, C.S., Ahmed, Z.E., Asma, A.A.H., Faheema, K.** Copper Nanoparticles: Green Synthesis and Managing Fruit Rot Disease of Chilli Caused by Colletotrichum Capsica *Saudi Journal of Biological Sciences* 28 (2) 2021: pp. 1477 – 1486. https://doi. org/10.1016/j.sjbs.2020.12.003
33. **Qiu, H., Feng, K., Gapeeva, A., Meurisch, K., Kaps, S., Li, X., Yu, L., Mishra, Y.K., Adelung, R., Baum, M.** Functional Polymer Materials for Modern Marine Biofouling Control *Progress in Polymer Science* 127 2022: pp. 101516. https://doi.org/10.1016/J. PROGPOLYMS CI. 2022. 101516